Control of iron(II)-tris(2,2'-bipyridine) light-induced excited-state trapping via external electromagnetic fields

M. Alías-Rodríguez,[*,a] M. Huix-Rotllant,[*,a]

Photoinduced spin crossover reactions in iron pyridinic complexes allow the iron's low-to-high spin transition in a sub-picosecond timescale. Employing a recently developed model for $[\text{Fe}(2,2'-\text{bipyridine})_3]^{2+}$ photochemical spin-crossover reaction in conjunction with quantum wavepacket dynamics, we explore the possibility of controlling the reaction through external electromagnetic fields, aiming at stabilizing the initial metal-to-ligand charge transfer states. We show that simple Gaussian-shaped electromagnetic fields have a minor effect on the population kinetics. However, introducing vibrationally excited initial wavepacket representations allow to maintain trapped the population into the metal-to-ligand charge transfer states. Using optimal control theory, we propose an electromagnetic field shape that increases the lifetime of metal-to-ligand charge transfer states. These results open the route for controlling the iron photochemistry through the action of external electric fields.

Introduction

Spin crossover (SCO) reactions in organometallic complexes are attractive for their potential applications in data storage, displays and molecular electronics, etc.[1] Among them, iron-based complexes attract a particular interest since providing a cost-effective and environmental-friendly metal substitution. There is a growing interest in controlling iron complexes photochemistry, especially for applications like photoredox catalysis.[2] An obvious strategy is to substitute nobel metals by iron keeping the archetypal polypyriyl complexes that act as photocatalysts.[2] However, despite the excellent photocatalytic activity of for example $[\text{Ru}(\text{bpy})_3]^{2+}$ (bpy=2,2'-bipyridine) due to a trapping of in metal-to-ligand charge transfer (MLCT) states for 580 ns,[3,4] $[\text{Fe}(\text{bpy})_3]^{2+}$ undergoes an ultrafast sub- picosecond low- to high-spin conversion upon light absorption with no catalytic activity.[5,6] Understanding the photochemical mechanisms of iron complexes is therefore fundamental for controlling their reactivity in the excited state through chemical substitution. Despite the intense research on the well-known examples like $[\text{Fe}(\text{bpy})_3]^{2+}$, their light-induced excited spin-state trapping (LIESST) reaction mechanism has been a matter of intense debate for both theoretical and experimental literature.[7-22] In $[\text{Fe}(\text{bpy})_3]^{2+}$, light absorption to the lowest-energy bright singlet metal-to-ligand charge transfer (MLCT) triggers a quantum nuclear wavepacket that rapidly converts into triplet MLCT in a sub-50 fs process.[11,21,22] Concomitantly, a $^3\text{MLCT}{\rightarrow}^3\text{T}_1$ internal conversion to the triplet metal-centered (MC) states happens in around 100-150 fs after photon absorption.[10,12,13,21,22] In the MC state, the intersystem crossing to the lowest high spin state ($^5\text{T}_2$) starts to build up after 50 fs and a kinetic constant of around 250 fs.[10,12,13,21,22]

Long-lived MLCT state in iron complexes have been mainly pursued by designing new ligands. Such approach has shown an increase of the lifetime of MLCT states from tens of ps up to few nanosecond with respect to the sub-ps decay of $[\text{Fe}(\text{bpy})_3]^{2+}$.[21,23-27] Here, we explore an alternative route for trapping the excited state lifetime by employing shaped laser pulses.[28] Indeed, a tailored laser pulse can maximize the population on certain electronic states. For the particular case of $[\text{Fe}(\text{bpy})_3]^{2+}$, photocatalytic activity of any iron complex could be attained by a laser pulse that blocks the evolution of quantum nuclear wavepackets to the unreactive MC states of iron that rapidly evolves to the quintets. For this purpose, we develop a quantum wavepacket dynamics model of $[\text{Fe}(\text{bpy})_3]^{2+}$ (with an extremely short MLCT lifetime) under laser fields. The model is based on the recently model hamiltonian for spin crossover developed in Ref. 21. We explore first the effect on the quantum dynamics from a wavepacket prepared from a pump Gaussian-shaped laser pulse excitation on the MLCT band. We then explore the effect of an initial vibrational excitation prior to the Gaussian pump laser. Finally, we employ optimal control theory to design a laser that allows the trapping of the excited state population.[29,30]

Methodology

Multi-configuration time-dependent Hartree

We employed the multi-configuration time-dependent Hartree (MCTDH) method to perform the wavepacket quantum dynamics. This is widely explained in the literature[31] and only a brief explanation will be given here. MCTDH is based on the following wave function *ansatz* to solve the time-dependent Schrödinger equation.

$$\Psi(q_1, ..., q_f, t) = \sum_J A_J(t)\Phi_J(q_1, ..., q_f, t) \qquad (1)$$

where f are the degrees of freedom for the system, J is a composite index $J = j_1...j_f$, A_J are the time-dependent coefficients and Φ_J the time and coordinate-dependent Hartree products of single-particle-functions (SPFs).

[a] Dr. M. Alías-Rodríguez*, Dr. M. Huix-Rotllant*
Aix-Marseille Univ, CNRS, ICR, 13013 Marseille, France
E-mail: marc.alias-rodriguez@univ-amu.fr
miquel.huix-rotllant@cnrs.fr

$$\Phi_J = \prod_{k=1}^{f} \varphi_{jk}(Q_k, t) \qquad (2)$$

At the same time, the SPFs are formed by linear combinations of primitive basis, called discrete variable representation (DVR). The DVR corresponds to the lowest energy solutions of the harmonic oscillator of each coordinate.

$$\varphi_j^{(k)}(Q_k, t) = \sum_{k=1}^{n_k} a_{kj}^{(k)}(t) \chi_j^{(k)}(Q_k) \qquad (3)$$

The multi-set formalism has been used to study the different electronic states. In this approach, a different wave function is employed for each electronic state.

$$\Psi(q_1, q_2, ..., \alpha, t) = \sum_{\alpha=1}^{\sigma} \Psi^{(\alpha)} |\alpha\rangle \qquad (4)$$

where α runs over the different electronic states.

This allows a more efficient wave function because SPFs adapt better to each electronic state and fewer configurations are necessary.

Model Hamiltonian for the Fe(bpy)$_3$ photoinduced spin crossover

We used the 9D model Hamiltonian including the main vibrational modes of $[Fe(bpy)_3]^{2+}$ generated in our previous study.[21] Figure 2 shows the set of vibrational modes that is formed by the reaction coordinate, a combined mode connecting the LS and HS minima, two Fe-N asymmetric stretching, and six high-frequency modes associated to stretchings on the bipyridine units. In the model, we included the lowest 13 singlets (GS, 9 MLCT and 3MC states), 15 triplets (6MC and 9 MLCT states), and 3 quintets. The model Hamiltonian is described as follows:

$$\hat{H}(q) = \hat{T}_N(q)\mathbf{1}_n + \hat{V}(q) \qquad (5)$$

where $\hat{T}_N$ is the nuclear kinetic energy, $\mathbf{1}_n$ is the unit matrix of n-dimension (n being the number of electronic states) and $\hat{V}$ contains the potential of the electronic states along each mode and the couplings among them.

The nuclear kinetic energy operator is a diagonal operator, with the following shape in mass-frequency weighted coordinates

$$\hat{T}_N = -\sum_i \frac{\omega_i}{2} \frac{\partial^2}{\partial q_i^2} \qquad (6)$$

where ω_i is the ground state frequency for each normal mode. The potential $\hat{V}$ is defined in a diabatic basis as
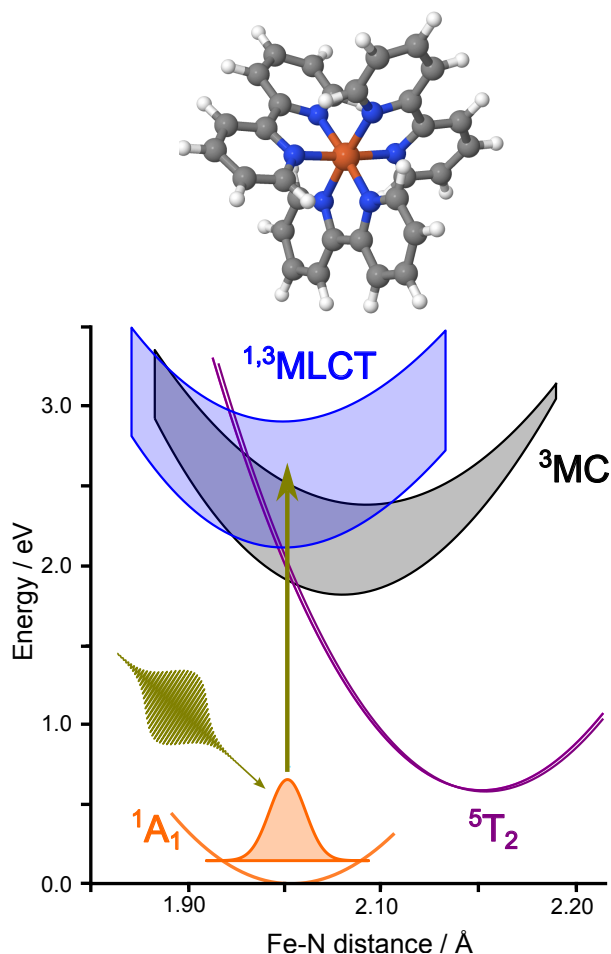
$$\hat{V}(q) = \sum_{nn'} \left(V^{nn}(q)\delta_{nn'} + V_{NAC}^{nn'}(q) + V_{SOC}^{nn'} \right) |n\rangle\langle n'| \quad (7)$$

The diagonal term of the potential operator is described as

$$V^{nn}(q) = E_n + \sum_i \left(\kappa^{n,i} q_i + \frac{\lambda^{n,i}}{2!} q_i^2 + \frac{\mu^{n,i}}{3!} q_i^3 + \frac{\gamma^{n,i}}{4!} q_i^4 \right) \qquad (8)$$

where $\kappa^{n,i}$, $\lambda^{n,i}$, $\mu^{n,i}$ and $\gamma^{n,i}$ are the linear, quadratic, cubic, and quartic terms, respectively, for state n along mode i.

The off-diagonal terms of the Hamiltonian are split into non-adiabatic couplings (NACs) and spin-orbit couplings (SOCs).

Figure 1. (top) Schematic representation of the $[Fe(bpy)_3]^{2+}$ structure in the ground state; (bottom) Diabatic potential energies along the reaction coordinate. Singlet and triplet ^{1,3}MLCT states are represented as bands in blue, the $^1A_1$ is drawn in orange, ^{3}MC in black, and HS in purple. The electric field (yellow) drives the wavepacket in the ^{1}MLCT band.
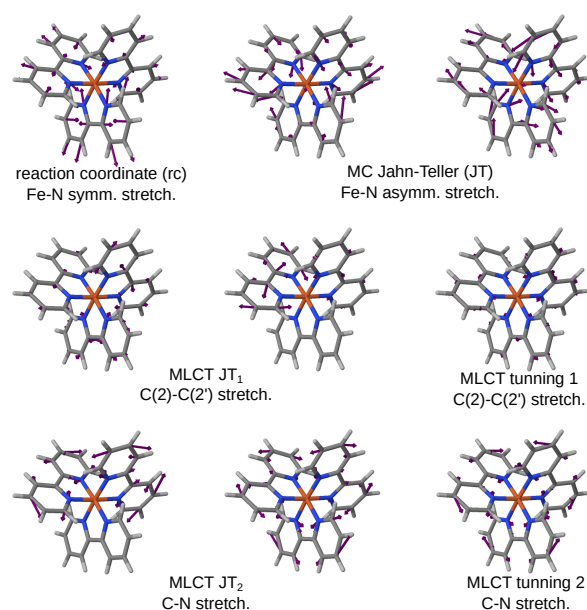
Figure 2. Representation of the vibrational modes included in the model Hamiltonian.

2

$$V_{SOC}^{nn'} = \langle n| \hat{H}^{SO} |n'\rangle \qquad (9)$$

$$V_{NAC}^{nn'}(q) = \sum_i \alpha_i^{nn'} q_i \qquad (10)$$

The $V_{SOC}^{nn'}$ are the coordinate-independent terms couplings singlets, triplets, and quintets. The diabatic potential, V^{nn}, and the $V_{NAC}^{nn'}$ are coordinate-dependent parameters obtained by a fitting procedure of the adiabtic surfaces within each spin multiplicity. Further information about the construction of the model Hamiltonian may be found in Ref. 21.

Radiation external field

The light-matter interaction term for the semiclassical Hamiltonian within the dipole approximation is described as

$$H_{FLD}^{nn'} = -\vec{\mu}_{nn'} \cdot \vec{E}(t) \qquad (11)$$

where $\vec{\mu}_{ij}$ is the transition dipole moment vector between the pair of states i and j, and $\vec{E}(t)$ is the time-dependent electric field vector. This term is added to the model Hamiltonian defined in Eq. 5. Two different definitions of the time-dependent electric field have been employed. The simplest electric field considers a constant frequency corresponding to the excitation energy of the bright states,

$$\vec{E}(t) = \vec{E}_0 e^{-t^2/2\sigma^2} cos(\frac{2\pi}{T_0}t) \qquad (12)$$

where the initial electric field is set to $\vec{E}_0 = (0.079, 0.079, 0)$ in a.u., T_0 is 1.56 fs, the period associated to the energy of S_7 and S_8 and σ is 5 fs, a parameter to modulate the laser attenuation. In addition, we consider the effect of a chirped electric field with varying ressonant frequency,

$$\vec{E}^{chirp}(t) = \vec{E}_0 e^{-t^2/2\sigma^2} \left(\Theta(t)cos(\omega_1(t)t) + \Theta(-t)cos(\omega_2(t)t)\right) \qquad (13)$$

in which $\omega_1(t) = \frac{2\pi}{T_0} + [\frac{2\pi}{T_1} - \frac{2\pi}{T_0}]e^{(-t/p_3)^2}$ and $\omega_2(t) = \frac{2\pi}{T_0} + [\frac{2\pi}{T_2} - \frac{2\pi}{T_0}]e^{(-t/p_3)^2}$. Here, T_1 and T_2 are the periods associated with the waves with a wavelength of $\pm$ 20 nm with respect to T_0, $\theta(t)$ and $\theta(t)$ are the Heaviside and reverse Heaviside step functions, respectively.

The plots of the time-dependent electric-field in the time and frequency regimes are shown in Figure S2 of the supporting information.

Computational details

The dynamics are run using MCTDH (8.4.21 version of Heidelberg package).[32] The multi-set formalism was employed to more accurately represent the flexibility for each state in the model. Table 1 summarize the set-up used for the simulation, i.e. the number of SPFs for each electronic state in each mode grouped by their spin-multiplicity (singlet, triplet or quintet) and character (MLCT or MC), the number of primitive basis and the grid along each mode. Detailed information about the obtaining of the parameters for the model Hamiltonian may be found in the Supporting Information of our previous work.[21]

In the last section, we optimised a laser to maximize the population of the MLCT states. To this aim, we have used the optimal control formalism implemented in MCTDH package.[33] The target function is the population of the ^{1}MLCT

Table 1. Set-up of the MCTDH simulation: n_i represent the number of primitive basis functions, the grid limits are expressed in adimensional MFWC and N_i are the number of SPFs for each electronic state. Modes combined are represented together.

Mode	n_i	Grid lim.		N_i		
				$^1A_1$ / MLCT	^{3}MC	$^5T_2$
RC	73	-4.0	20.0	5	10	25
MC JT	49	-6.0	6.0	10	10	10
	49	-6.0	6.0			
MLCT JT$_1$	25	-4.0	4.0	10	10	10
	25	-4.0	4.0			
MLCT t.$_1$	25	-4.0	4.0	4	4	4
MC JT$_2$	25	-4.0	4.0	10	10	10
	25	-4.0	4.0			
MLCT t.$_2$	25	-4.0	4.0	4	4	4

states, which is maximized at 50 fs varying the electric field and using as initial guess the chirped electric field employed in the previous calculations. The optimization is computationally demanding, therefore, we did it in a reduced model without including the quintet states and using a smaller nuclear basis set with only 3 SPFs for each electronic state along each mode. The electric field obtained is used afterwards in the complete model using a nuclear basis set of 5 SPFs for each electronic state in reaction coordinate and Jahn-Teller modes and 4 SPFs for the tunning modes.

Results and Discussion

Results are divided in three sub-sections. In the following section, we will study the effect of an initial vibrational excitation prior to the UV-visible excitation. Finally, we will employ optimal control to efficiently design lasers to maximize the population on the MLCT band and the HS state.
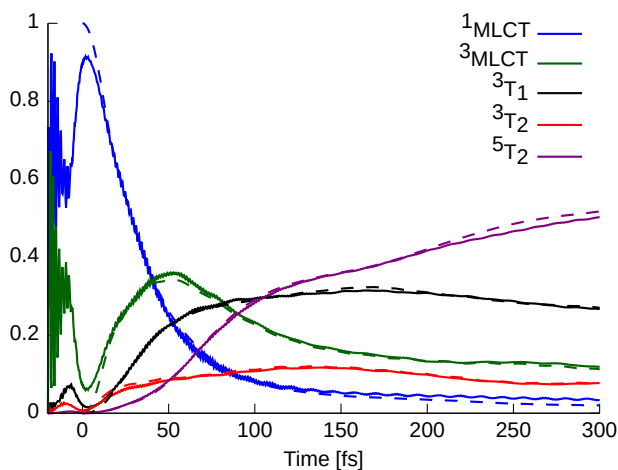
Laser effect on photodynamics of Fe(bpy)$_3$

Here, we include a UV/vis laser pump pulse to determine the effect on the ultrafast SCO mechanism of Fe(bpy)$_3$. In a previous study, we studied this mechanism by directly placing a wavepacket in the excited state as initial condition (delta pulse).[21] The dynamics were started from the lowest-energy singlet MLCT bright states. The proposed deactivation pathway occurs in a sequential mechanism: ^{1}MLCT$\rightarrow$^{3}MLCT$\rightarrow$^{3}MC$\rightarrow$$^5T_2$. The population from ^{1}MLCT states was rapidly transferred to the ^{3}MLCT band in less than 50 fs. Subsequently, population of ^{3}MC states occur mainly via internal conversion (IC) from ^{3}MLCT and also via intersystem crossing (ISC) from ^{1}MLCT to a lesser extend. The ^{3}MC population is finally transferred to $^5T_2$ state.[21]

In the first step of the dynamics, the wavepacket placed in the ^{1}MLCT states evolves rapidly within the MLCT manifold. This process is assisted by the high-frequency modes, which are C-C and C-N stretchings in the bipyridine ligands. These modes are activated to stabilize the extra negative charge on the ligands transferred from the metal in the MLCT states. This allows a very fast cascade relaxation in a region of multiple crossings between states. Consequently,

the population of the ^{3}MC states grows concomitant to the decay of the MLCT band in the first 50 fs of the dynamics. Triplet MC states may receive population via IC and a smaller portion through the ISC directly from the ^{1}MLCT band. The ^{3}MC states exhibit an electron configuration with an electron in the e$_g$ orbitals, which have σ^* character along Fe-N bond. Population on these ^{3}MC states activate the reaction coordinate and MC JT modes because they affect Fe-N stretchings and may stabilize these states.

This dynamical mechanism could be affected depending on how the initial wavepacket is prepared. For this reason, we performed the simulations by explicitly including the laser pump. This is done by introducing an extra light-matter interaction term between the transition dipole moments and the external time-dependent electric field. Two different lasers are tested with our Fe(bpy)$_3^{2+}$ model. The first one is a "non-chirped" laser (see Eq. 12) with a fixed frequency tuned to correspond to the excitation energy of the bright singlet states. The second is a "chirped" laser pulse (see Eq. 13) with a varying frequency and an energy width of 40 nm centered at the same frequency as the "non-chirped" laser. Both lasers are enveloped with a Gaussian function with a time window of 40 fs, that increases the width of the lasers in the frequency domain (see Fig. S2 in the SI). The quantum dynamics simulations using the two different analytical lasers leads to nearly identical evolution of populations (Fig. S3 in SI). Hereafter, we will discuss only the chirped laser results. For the sake of comparison, we normalized the population on the excited states, excluding the population trapped in the singlet ground state.

Figure 3. Time-evolution diabatic population. ^{1}MLCT in blue, ^{3}MLCT in green, $^3T_1$ in black, $^3T_2$ in red, and $^5T_2$ in pink. Populations obtained after laser excitation (solid line) and kick excitation (dashed line) from Ref. 21.

In Figure 3, we compare the evolution of the populations with and without laser pulse. Overall, the evolution of the diabatic population is nearly identical using a delta or a laser excitation, which indicates the minor effect of the laser in the photodynamics, despite the initial condition at the initial time is noticeably different. For the delta pulse, the quantum dynamics simulation starts at time zero, at which all the population is placed at ^{1}MLCT states. In the laser excitation, the time 0 is set at the maximum strength of the time-dependent electric field. At negative times, large oscillations between singlet and triplet MLCT state populations

are observed. This is because the population is normalized with respect to the population transferred to the excited states, which is residual at the initial time. The population of the ^{1}MLCT is around 90% at the initial time. This can be interpreted in two different ways: (i) part of the population is promoted to the ^{1}MLCT at earlier times which is subsequently transferred triplet states producing the mentioned picture; (ii) the presence of spin-orbit coupling in our model leads to spin-mixed states, that can be populated directly via dipole moment.
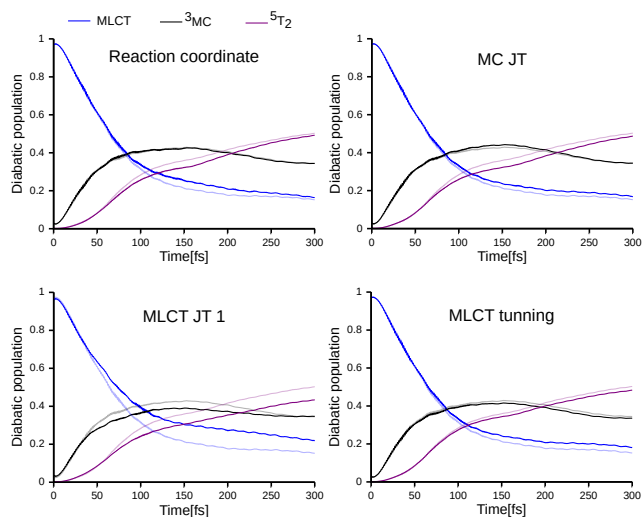
Effect of vibrationally excited wavepackets

In the previous section, the initial wavepacket was represented as the lowest-energy wavefunction of a quantum harmonic oscillator along each normal mode. This leads to a Gaussian-shaped wavepacket for each coordinate. In this section, we investigate the effect of using first excited states of the quantum harmonic oscillator, that is, the wavepacket exhibits a node at the distance origin. Such quantum dynamics simulations would thus correspond to an initial vibrational infrared or Raman pump followed by the UV pump that allows the electronic excitation from the electronic ground state (for the infrared and Raman spectra of Fe(bpy)$_3^{2+}$, see Figure S1 of the supporting information). Our target here is to trap the population on the MLCT band. For this reason, we sum up the ^{1}MLCT and ^{3}MLCT populations (labeled as MLCT), and the metal-centered triplets $^3T_1$ with $^3T_2$ (labeled as ^{3}MC).

Figure 4 shows the evolution of population from quantum dynamics starting from an initially wavepacket in which one vibrational mode is excited at a time. We include modes of different types such as reaction coordinate, Jahn-Teller modes for MC and MLCT states and MLCT tuning modes. The complete set of population evolutions from the dynamics excited each vibrational mode can be found in the supporting information (Fig. S4-S12).

For the reference calculations, the initial steps of the photoprocess are governed by the relaxation within the MLCT band, mainly assisted by the C-C and C-N stretching modes on the bipyridine ligands. Therefore, a small effect is expected after vibrational excitations on the reaction coordinate or MC Jahn-Teller in the evolution of the MLCT population. On the contrary, an important effect is foreseeable when exciting MLCT JT or MLCT tuning modes. After the transfer from the MLCT band to the ^{3}MC states, the latter relax along the reaction coordinate and Jahn-Teller modes, where there is an effective crossing towards the $^5T_2$ state. Consequently, we could hope a variation in this second transfer, at larger time scales, when exciting reaction coordinate or MC JT modes.
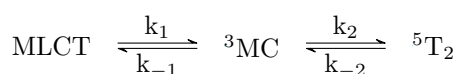
The vibrational excitation of the reaction coordinate or the MC JT modes has almost no effect on the dynamics, leading to the same evolution of the population as the reference calculation. There is only a variation at 150 fs with respect to the reference, in which the population of the MLCT band and ^{3}MC states are slightly larger and the $^5T_2$ slightly smaller. The population trapped into the ^{3}MC states acts as a bottleneck, blocking the transfer from the MLCT band. We attribute this to the excess of kinetic energy along these modes decrease the lifetime in the ^{3}MC minimum, where the crossing towards quintet states is more efficient. This effect is more important for the excitation of the reaction coordinate than in MC JT mode because the former relaxes the ^{3}MC states and the formation of the high-spin state.

4

Figure 4. Time-evolution diabatic population from the vibrationally excited state (solid lines) and from the vibrationally ground state (transparent line). The dynamics represent the excitation in the reaction coordinate (top-left), MC Jahn-Teller (top-right), MLCT Jahn-Teller (bottom-left) and MLCT tunning (bottom-right). All the excitations have been carried out to the first vibrational excited state.

At variance with the reaction coordinate and MC JT mode excitation, the vibrational excitation of an MLCT JT mode exhibits important differences with respect to the reference simulations. Starting at 50 fs, we observe a larger populationin the MLCT band and a lower population transfer to the ^{3}MC and HS states with respect to the reference. Such modes are fundamental for the relaxation of the wavepacket within the MLCT band and the consequent transfer to the triplet MC states. The larger amount of kinetic energy difficults to reach that region and cause a higher lifetime in the MLCT states. However, the excitation in the MLCT tunning mode has a small effect in the population trapped in the MLCT band. There is only a slight increase in the population on the MLCT band at larger times. This seems to indicate that the tuning modes play a minor role in the relaxation of the MLCT band and they may only have a small influence in the transfer of the remaining population from the band at larger simulation times.

$$ \text{MLCT} \quad \underset{k_{-1}}{\overset{k_1}{\rightleftharpoons}} \quad {}^3\text{MC} \quad \underset{k_{-2}}{\overset{k_2}{\rightleftharpoons}} \quad {}^5\text{T}_2 $$

Figure 5. First order kinetic mechanism considered for the fitting of the diabatic population evolution in the full model Hamiltonian.

To quantify the effect on the dynamics, we fitted the evolution of populations to the following first order kinetic mechanism shown in Fig. 5. The results for the time constants ($\tau = 1/k$) are summarized in Table 2. For the first part of the photoreaction, the population will get more trapped on the MLCT band when the time constant of τ_1 increases and the time constant of the inverse reaction τ_{-1} is decreased. For the second part of the photoreaciton, the transfer from the ^{3}MC states to the HS state is faster with a small τ_2 and a large time constant for the inverse reaction τ_{-2}. These time constants show that simulations starting from a vibrationally excited state increase the lifetime of the MLCT states.

From the population evolution, we observed that the amount

of population trapped in the MLCT band is larger when the excitation is on the Jahn-Teller vibrational modes centered on the bipyridine ligands. This trapping is not due to change in τ_1 (nearly identical for all simulations) that controls the MLCT to MC transfer, but rather due to a faster back-transfer from the MC to the MLCT band (decreased τ_{-1}). Such effect is more important for the MLCT tunning mode, where the difference with respect to the reference occurs at even larger time scale. From the second part of the photoreaction, there is little effect of the vibrational excitations of the wavepacket on the kinetic reates of transfer from the ^{3}MC to the ^{5}T$_2$ states, comparing well with the reference kinetic rates.

Table 2. Time constants (in fs) with the different initial excitations.

	ref.	RC	MC JT	MLCT JT$_1$	MLCT t$_1$	v$^*_{mod}$
τ_1	83	85	84	89	82	127
τ_{-1}	316	264	268	170	227	82
τ_2	82	99	99	79	84	69
τ_{-2}	116	148	138	97	117	44
* v$_{mod}$=[0,0,0,1,1,1,1,1,1].						
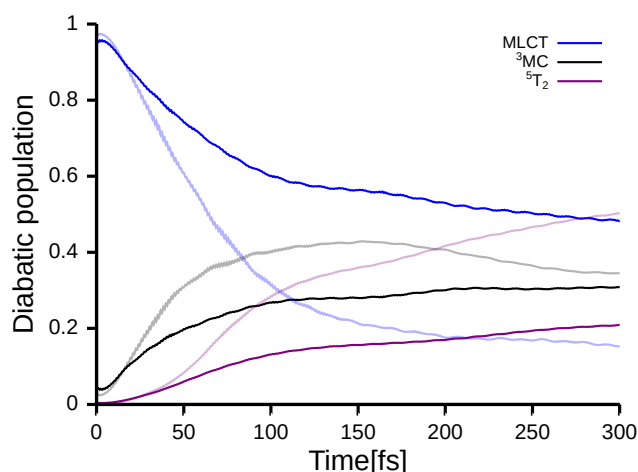
Figure 6. Time-evolution diabatic population from the v$_{mod}$=[0,0,0,1,1,1,1,1,1] vibrationally excited state (solid lines) and from the vibrationally ground state (transparent line).

We conclude this section by performing a wavepacket simulation in which several vibrational modes are excited simultaneously as a combination band. These simulations are shown in Figure 6, where the initial vibrational wavepacket is prepared on the first excited state in all the bipyridine vibrational normal modes (further details may be found in the SI (Fig. S13-S14)). We observe that the increase of MLCT population observed for each mode separately is actually additive. In this simulation, the transfer from the MLCT band rapidly decrease and almost half of the population remain trapped in the MLCT band at 300 fs. Consequently, the population in the ^{3}MC and ^{5}T$_2$ is much smaller than in the vibrationally ground state simulations. These results are also quantified in terms of time constants in Table 2. The combination band exhibits the larger τ_1 and the smaller τ_{-1} for the inverse reaction. These promising results may

open a new route to achieve long-lived MLCT states in iron complexes.

## Optimal control designed electric field

In this final section, we employ optimal control theory to optimise a time-dependent electric pulse that can trap the population in the MLCT band. This would extend the applicability of current iron-based organometallic complexes for photocatalytic applications, without the need to chemically modify the structure. The optimized a time-dependent electric field as well as the evolution of populations under such a field are shown in Figure 7. The optimized target is a function of the parameters of the field that maximize the population of the ^{1}MLCT states. For the sake of simplicity, we allowed the field to act on the first 50 fs of the dynamics. The initial field is a Gaussian-shaped chirped laser with the same parameters as described in the previous sections. For these simulations, we employed a reduced model Hamiltonian only containing the MLCT band and the ^{3}MC states. The field has some initial grow of intensity up to 20 fs, and a progressive lose of intensity up to 50 fs. Fourier transform of the optimised laser is shown in Fig. S15. This is formed by multiple frequencies between 0 and 3.5 eV. However, the region around 3 eV shows slightly larger intensities which coincides with the excitation energies of the bright MLCT states (2.65 eV).

The evolution of electronic excited states population during the first 100 fs under the optimized electric field is shown in Fig. 7. The laser is optimised for the first 50 fs and then the laser is turned off. The decay in the MLCT band population is slower when the laser is active than in the reference. At 50 fs, the population in the MLCT band is a 5% higher in the optimized laser (excluding in both cases the population in the ground state). However, once the laser is deactivated the transfer from the MLCT band to the triplet manifold is accelerated. At 100 fs, the difference in the MLCT band population is lower than 2% between the optimised laser and the reference. Despite the population in the MLCT band is slightly increased when excluding population trapped in the ground state, we observe that population remaining in the ground state is about 8% in the optimised laser, while in the reference simulation was higher than 58%. Therefore, most of the population gained for the MLCT band during the optimization process comes from the ground state.

Conclusion

In this study, we have determined the effect on the photodynamics of Fe(bpy)$_3$ of using several time-dependent electric fields representing a UV/visible laser pump or a IR/Raman pump combined with a UV/visible pump. The UV/visible pump produce a wavepacket on the bright ^{1}MLCT band. We observe that such photodynamics gives a similar kinetic evolution of populations than the more simpler delta pulse used in most common quantum dynamics simulations of iron complexes. This indicates that the laser is neither changing the shape of the initial wavepacket, nor preparing a wavepacket on a coherent superposition of states that could significantly affect the photodynamics.

We have shown that a combination of IR/Raman pump pulse prior to the UV/visible pump pulse significantly changes de photoprocess, and is able to trap the population in the MLCT. Indeed, the use of a vibrationally excited wavepacket
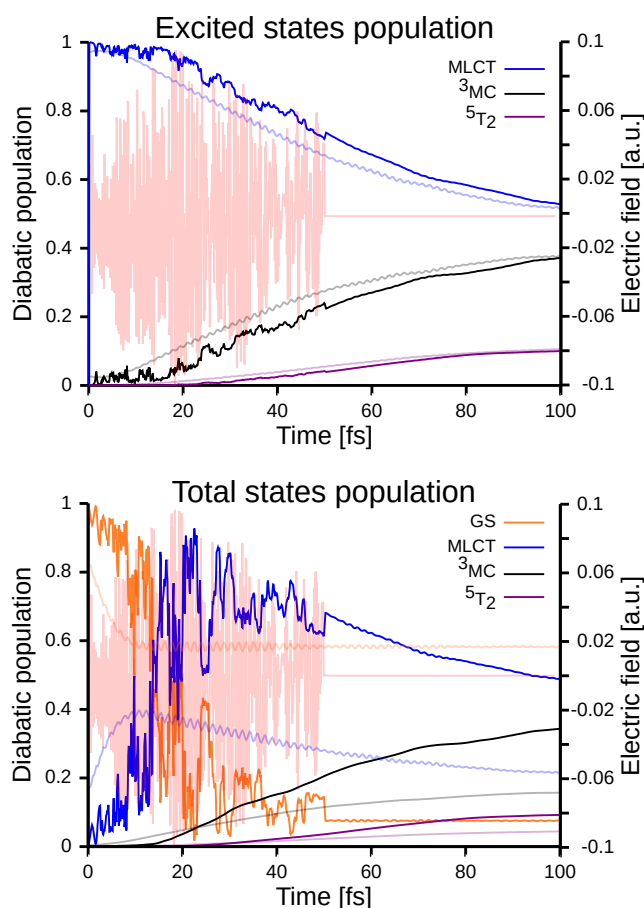
Figure 7. Time-evolution of the diabatic population only including excited states (top) and including also the ground state (bottom). Reference diabatic populations from the initial vibrational ground state is shown in full-color solid line for the ground-state (orange), triplet metal-centered state (black), metal-ligand charge transfer (blue) and high-spin state (magenta) on the left y-axis. The time-dependent electric field is represented in red semi-transparent line on the right y-axis.

in the high-frequency modes blocks the transfer from the MLCT band. Consequently, a multiple excitation to several ligand modes in a combination band could be used as a way to increase the lifetime of MLCT states in any iron complexes.

Optimal control theory is an alternative way to trap population in the MLCT band by tuning an electric field that maximizes the population in such excited states. Despite observing indeed a traping in the presence of the laser, when it is turned off the population is transfered back to the higher spin states following the usual photodynamics. This probably indicates that the laser pulse should be continuously switched on in order to trap the population for longer times.

In conclusion, the trapping of population in metal-ligand charge-transfer states in Fe(bpy)$_3$ is possible either by combining IR/Raman and UV/vis pumps or by a specially designed UV/vis pump. This opens up the route for converting iron spin crossover complexes in photocatalysts by action of external electric fields.

Acknowledgements

Conflict of Interest

Please enter any conflict of interest to declare.

References

[1] J.-F. Létard, P. Guionneau, L. Goux-Capes, Towards Spin Crossover Applications, page 221249, Springer-Verlag.

[2] L. H. M. de Groot, A. Ilic, J. Schwarz, K. Wärnmark, Journal of the American Chemical Society **2023**, 145, 9369.

[3] S. F. McClanahan, J. R. Kincaid, Journal of the American Chemical Society **1986**, 108, 3840.

[4] P. Dongare, B. D. Myron, L. Wang, D. W. Thompson, T. J. Meyer, Coordination Chemistry Reviews **2017**, 345, 86, chemical Bonding: "State of the Art".

[5] P. Gütlich, H. A. Goodwin, Spin Crossover—An Overall Perspective, pages 1–47, Springer Berlin Heidelberg, Berlin, Heidelberg **2004**.

[6] R. W. Hogue, S. Singh, S. Brooker, Chem. Soc. Rev. **2018**, 47, 7303.

[7] W. Gawelda, A. Cannizzo, V.-T. Pham, F. van Mourik, C. Bressler, M. Chergui, J. Am. Chem. Soc. **2007**, 129, 8199.

[8] C. Bressler, C. Milne, V.-T. Pham, A. ElNahhas, R. M. van der Veen, W. Gawelda, S. Johnson, P. Beaud, D. Grolimund, M. Kaiser, C. N. Borca, G. Ingold, R. Abela, M. Chergui, Science **2009**, 323, 489.

[9] A. Cannizzo, C. Milne, C. Consani, W. Gawelda, C. Bressler, F. van Mourik, M. Chergui, Coord. Chem. Rev. **2010**, 254, 2677.

[10] W. Zhang, R. Alonso-Mori, U. Bergmann, C. Bressler, M. Chollet, A. Galler, W. Gawelda, R. G. Hadt, R. W. Hartsock, T. Kroll, K. S. Kær, K. Kubič, H. T. Lemke, H. W. Liang, D. A. Meyer, M. M. Nielsen, C. Purser, J. S. Robinson, E. I. Solomon, Z. Sun, D. Sokaras, T. B. van Driel, G. Vankó, T.-C. Weng, D. Zhu, K. J. Gaffney, Nature **2014**, 509, 345.

[11] G. Auböck, M. Chergui, Nat. Chem. **2015**, 7, 629.

[12] H. T. Lemke, K. S. K. R. Hartsock, T. B. van Driel, M. Chollet, J. M. Glownia, S. Song, D. Zhu, E. Pace, S. F. Matar, M. M. Nielsen, M. Benfatto, K. J. Gaffney, E. Collet, M. Cammarata, Nat. Commun. **2017**, 8, 15342.

[13] K. S. Kjær, T. B. V. Driel, T. C. B. Harlang, K. Kunnus, E. Biasin, K. Ledbetter, R. W. Hartsock, M. E. Reinhard, S. Koroidov, L. Li, M. G. Laursen, F. B. Hansen, P. Vester, M. Christensen, K. Haldrup, M. M. Nielsen, A. O. Dohn, M. I. Pápai, K. B. Møller,

P. Chabera, Y. Liu, H. Tatsuno, C. Timm, M. Jarenmark, J. Uhlig, V. Sundstöm, K. Wärnmark, P. Persson, Z. Németh, D. S. Szemes, É. Bajnóczi, G. Vankó, R. Alonso-Mori, J. M. Glownia, S. Nelson, M. Sikorski, D. Sokaras, S. E. Canton, H. T. Lemke, K. J. Gaffney, Chem. Sci. **2019**, 10, 5749.

[14] M. Oppermann, F. Zinna, J. Lacour, M. Chergui, Nat. Chem. **2022**, 14, 739.

[15] C. de Graaf, C. Sousa, Chem. Eur. J. **2010**, 16, 4550.

[16] A. Domingo, C. Sousa, C. de Graaf, Dalton Trans. **2014**, 43, 17838.

[17] C. Sousa, C. de Graaf, A. Rudavskyi, R. Broer, J. Tatchen, M. Etinski, C. M. Marian, Chem. Eur. J. **2013**, 19, 17541.

[18] C. Sousa, M. Llunell, A. Domingo, C. de Graaf, Phys. Chem. Chem. Phys. **2018**, 20, 2351.

[19] L. C. Liu, Photoinduced Spin Crossover in Iron(II) Systems, pages 105–161, Chemistry in Action: Making Molecular Movies with Ultrafast Electron Diffraction and Data Science, Springer International Publishing, Cham, Switzerland **2020**.

[20] M. Alías-Rodríguez, M. Huix-Rotllant, C. de Graaf, Faraday Discuss. **2022**, 237, 93.

[21] M. Alías-Rodríguez, S. Bhattacharyya, M. Huix-Rotllant, The Journal of Physical Chemistry Letters **2023**, 14, 8571, pMID: 37725036.

[22] A. Lee, M. Son, M. Deegbey, M. D. Woodhouse, S. M. Hart, H. F. Beissel, P. T. Cesana, E. Jakubikova, J. K. McCusker, G. S. Schlau-Cohen, Chem. Sci. **2023**, 14, 13140.

[23] L. A. Fredin, M. Pápai, E. Rozsályi, G. Vankó, K. Wärnmark, V. Sundström, P. Persson, The Journal of Physical Chemistry Letters **2014**, 5, 2066.

[24] L. Liu, T. Duchanois, T. Etienne, A. Monari, M. Beley, X. Assfeld, S. Haacke, P. C. Gros, Phys. Chem. Chem. Phys. **2016**, 18, 12550.

[25] S. M. Fatur, S. G. Shepard, R. F. Higgins, M. P. Shores, N. H. Damrauer, Journal of the American Chemical Society **2017**, 139, 4493.

[26] K. Kunnus, L. Li, C. J. Titus, S. J. Lee, M. E. Reinhard, S. Koroidov, K. S. Kjær, K. Hong, K. Ledbetter, W. B. Doriese, G. C. O'Neil, D. S. Swetz, J. N. Ullom, D. Li, K. Irwin, D. Nordlund, A. A. Cordones, K. J. Gaffney, Chem. Sci. **2020**, 11, 4360.

[27] J. D. Braun, I. B. Lozada, C. Kolodziej, C. Burda, K. M. E. Newman, J. van Lierop, R. L. Davis, D. E. Herbert, Nature Chemistry **2019**, 11, 11441150.

[28] D. Keefer, R. de Vivie-Riedle, Accounts of Chemical Research **2018**, 51, 2279.

[29] D. J. Tannor, V. Kazakov, V. Orlov, Control of Photochemical Branching: Novel Procedures for Finding Optimal Pulses and Global Upper Bounds, pages 347–360, Springer US, Boston, MA **1992**.

[30] C. Gollub, M. Kowalewski, R. de Vivie-Riedle, Phys. Rev. Lett. **2008**, 101, 073002.

[31] G. A. Worth, H.-D. Meyer, H. Köppel, L. S. Cederbaum, I. Burghardt, International Reviews in Physical Chemistry **2008**, 27, 569.

[32] A. J. G. A. Worth, M. H. Beck, H.-D. Meyer, http://mctdh.uni-hd.de/ **2007**.

[33] M. Schröder, J.-L. Carreón-Macedo, A. Brown, Phys. Chem. Chem. Phys. **2008**, 10, 850.

Entry for the Table of Contents

8